JOURNAL OF GEOPHYSICAL RESEARCH, VOL. 95, NO. C9, PAGES 16,299–16,310, SEPTEMBER 15, 1990

Evidence of Bragg Scattering in Microwave Doppler Spectra of Sea Return

WILLIAM J. PLANT[1] AND WILLIAM C. KELLER

U.S. Naval Research Laboratory, Washington, D. C.

Microwave signals backscattered from the ocean (and one lake) have been collected at many different windspeeds and fetches. Doppler spectra of some signals obtained at low microwave frequencies exhibit double peaks clearly indicating Bragg scattering. At higher microwave frequencies, high wind speeds, long fetches, or in the presence of substantial swell, these splittings disappear. A model of microwave Doppler spectra based on Bragg-scattering, composite-surface theory is developed and used to show that the results obtained in these field studies are compatible with the hypothesis that Bragg scattering dominates microwave backscatter from rough water surfaces under many wind speed and incidence angle conditions. In particular, the model shows double peaks of the proper separation which disappear under the same conditions as those of the actual spectra. Furthermore, Doppler bandwidths given by the model agree with those of the field data under a variety of conditions. A rough angular dependence of the amplitudes of Bragg waves traveling in different directions with respect to the wind is deduced from the measurements. Finally, the implications of these findings for synthetic aperture radar imagery of the ocean are briefly discussed.

1. INTRODUCTION

Composite surface scattering theory was first introduced in the 1960s by *Wright* [1968] and *Bass et al.* [1968] to explain the features of backscattered microwave sea return which were known at that time. In the range of incidence angles from about 20° to 60° or 70°, the theory explained the polarization dependence of the return and yielded decent approximations of its intensity and Doppler bandwidths [*Wright*, 1968; *Valenzuela and Laing*, 1970; *Guinard et al.*, 1971]. In the years since these initial successes, composite surface- and Bragg-scattering ideas have received their strongest support from wave tank studies. They have been shown to yield estimates of the intensity of microwave return which agreed well with experiment for both paddle- and wind-generated waves [*Wright*, 1966; *Wright and Keller*, 1971; *Plant and Wright*, 1979]. Sharp Bragg resonance lines are routinely observed in Doppler spectra obtained in wind wave tanks and have been used to study mechanics of wind-generated waves such as their growth rates, phase speeds, and interactions [*Larson and Wright*, 1975; *Plant and Wright*, 1977, 1980; *Lee*, 1977].

In spite of these successes, questions still remain about the applicability and limitations of composite surface theory, especially in explaining microwave return under field conditions [*Kwoh and Lake*, 1983, 1984]. Part of the reason for this lingering concern is the fact that the theory is an approximate solution to the exact scattering equations which requires that surface slopes be small and that surface waves be reasonably divisible into short and long. Thus direct evidence supporting the applicability of such assertions must precede their acceptance. Such evidence is difficult to obtain in the field by simply observing received power levels because, according to the theory, these levels are proportional to the spectral density of the surface variance spectrum evaluated at the Bragg wave number. Although much work has been done to predict these spectral densities and their dependence on their environment, the measurement of variance spectra at high wave numbers by non microwave means is very difficult under field conditions [*Kitaigorodski*, 1983; *Phillips*, 1985; *Plant*, 1986]. At present, therefore, expected return power levels under various environmental conditions cannot be determined to an accuracy much better than a factor of 2 and therefore cannot exclude the possibility that other scattering mechanisms may be as important as Bragg scattering [*Plant*, 1986; *Durden and Vesecky*, 1985; *Donelan and Pierson*, 1987]. Note, however, that the polarization dependence of sea return is well established for the intermediate incidence angles specified above. Thus any alternate scattering theory must account for the higher level of return for vertically polarized radiation.

A more viable means of obtaining direct evidence of Bragg scattering from the ocean is to investigate the Doppler spectrum of the return. In the case of sea return observed at HF frequencies in the megahertz range, sharp first-order Bragg lines are prominent and provide solid evidence of the dominance of Bragg scattering at these frequencies. At microwave frequencies, however, Doppler spectra are generally broad and featureless, showing no peaks that could be interpreted as Bragg lines. In this paper we show that this is not always the case. Under certain field conditions, Bragg lines may be observed in microwave Doppler spectra. A model is developed based on composite surface theory and linear theory for long ocean waves which allows the prediction of the shape and bandwidth of microwave Doppler spectra under a variety of environmental conditions. Using this model, we show that observed Doppler spectra can be explained quite well up to perhaps 25-m/s wind speeds and that under most conditions encountered at sea, Bragg splittings are not to be expected in the spectra.

2. MODELING MICROWAVE DOPPLER SPECTRA

Composite surface theory decomposes a rough air-water interface into small-scale and large-scale features. Small-

[1]Now at Woods Hole Oceanographic Institution, Woods Hole, Massachusetts.

Paper number 89JC00787.

scale features may be highly irregular but are assumed to have small slopes and displacements. The irregular nature of this small-scale structure causes it to decorrelate very rapidly in time and space so that small segments, or facets, of this surface may be considered individually. Large-scale features are assumed to have curvatures small compared to the inverse of the small-scale decorrelation length so that they may be considered planar over these scales. Small-scale slopes and displacements are all measured relative to this large-scale surface. Thus the large-scale surface displaces correlated segments of the small-scale features, tilts them, and possibly changes their amplitude. Furthermore, any currents associated with the large-scale surface advect the segments of small-scale surface like corks floating on the large-scale surface.

Under these hypotheses, microwave scattering occurs because of resonant Bragg scattering from the small-scale surface. For backscatter, the resonant condition is

$$\lambda_B = \frac{\lambda_0}{2 \sin \theta_0} \tag{1}$$

where λ_0 is the microwavelength, λ_B is the short, Bragg-resonant wave responsible for the scatter, and θ_0 is incidence angle. Typical patterns from microwave antennas illuminate areas of ocean surface which are large compared with λ_B in both dimensions. In these conditions, only short waves propagating radially toward or away from the antenna backscatter to the antenna.

The standard equation for the Doppler shift, f_D, induced in backscattered microwaves due to a surface moving with a line-of-sight velocity v toward or away from the antenna is

$$f_D = \frac{2v}{\lambda_0} \tag{2}$$

If the scattering is a Bragg-resonant phenomenon as described above, then v is composed of the sum of any large-scale, line-of-sight velocities V and the component of the intrinsic phase speed, c, of the Bragg wave along the line of sight. Thus

$$v = V \pm c \sin \theta_0 \tag{3}$$

Combining equations (1), (2), and (3), Doppler shifts expected from composite surface theory are given by

$$f_D = \frac{2V}{\lambda_0} \pm f_B \tag{4}$$

where f_B is the intrinsic frequency of the Bragg-resonant short wave.

Thus for constant large-scale currents, or none at all, we expect a microwave Doppler spectrum due to Bragg backscattering to exhibit two sharp lines located at $\pm f_B$ corresponding to Bragg waves traveling toward or away from the antenna. The intensity of each line is proportional to the spectral density of the corresponding surface wave. Figure 1*a* shows that this is indeed the case for scattering in the wave tank where the Bragg wave is the dominant wave on the surface and large-scale structure is absent. The spectrum in Figure 1*a* is an *L* band (λ_0 = 16 cm) Doppler spectrum of backscatter from a surface roughened by a wind of friction velocity 28 cm/s. The fetch was 7.5 m, and the incidence

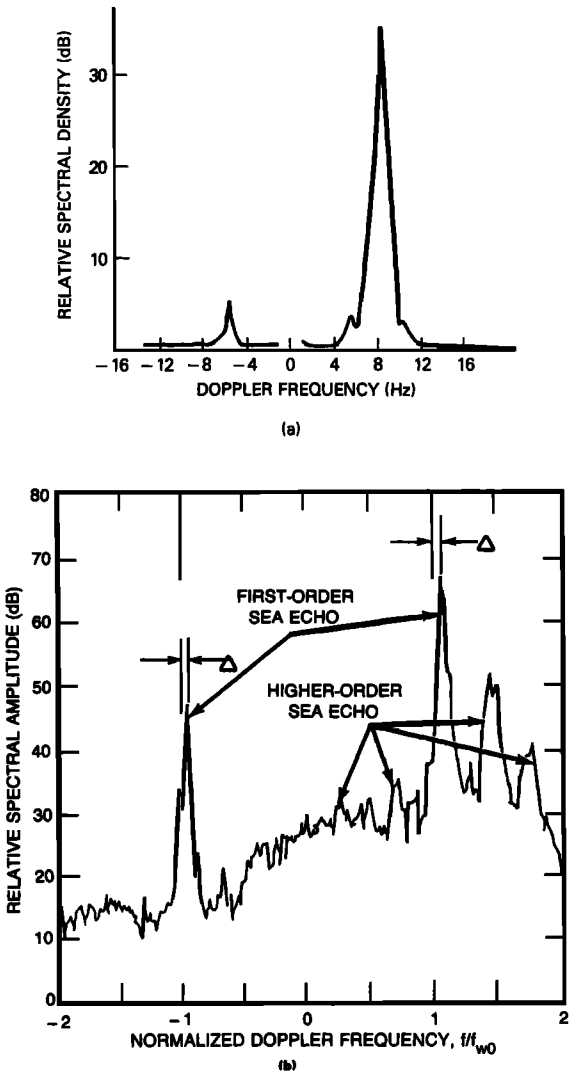

Fig. 1. (*a*) *L* band Doppler spectrum taken in a wind wave tank, where λ_0 = 16 cm, θ_0 = 54°, and wind friction velocity is 28 cm/s. (*b*) High-frequency Doppler spectrum from the ocean obtained at 9.4 MHz [from *Barrick et al.*, 1974]. In both figures, upwind Bragg waves have negative frequencies. The first-order Doppler shift f_{w0} = 0.31 Hz; Δ is an offset due to surface current.

angle was 54°. Note that the spectral density of the upwind traveling wave (negative frequency) is 3 orders of magnitude below that of the downwind travelling wave. Figure 1*b* shows that spectra exhibiting two Bragg lines, or "Bragg splitting," also occur routinely on the open ocean. This spectrum, taken from *Barrick et al.* [1974] is a high-frequency Doppler spectrum obtained at 9.4 MHz. For electromagnetic wavelengths corresponding to this frequency or lower ones, the dominant waves of the ocean are the small-scale structure while large-scale features must correspond to mesoscale circulation patterns.

The latter example points out the somewhat artificial nature of the division of scales on a composite surface–scattering model: wavelengths associated with small-scale and large-scale structure depend on the electromagnetic wavelength and incidence angle being used. A satisfactory dividing point is found to be a wavelength between 5 and 10 times as long as the Bragg wavelength. Thus to apply composite surface theory properly, a wave of

length 30 cm must be considered part of the large-scale structure when $\lambda_B = 3$ cm. As a result, the large-scale waves which advect the Bragg scatterers must be considered to be of two types [*Hasselmann et al.*, 1985]. Waves long compared with the resolution cell of the particular microwave system being considered (called long waves in the following) may be assumed to be constant over the cell. Then their effect on the Doppler spectrum results from their temporal variation over the time during which a spectrum is computed. On the other hand, intermediate-scale surface waves that are longer than the Bragg wavelength but smaller than the resolution cell (intermediate waves hereinafter) produce broadening of the spectrum due to their spatial variation within the cell. These waves must be treated statistically, since all spatially variable velocities produced by them affect the microwave signal at any instant of time. For many ocean conditions, the velocities produced by the orbital motions of these two classes of large-scale surface waves broaden the Bragg lines by more than their separation, causing the lines to be unresolved. Also, as Figure 1 indicates, many times one line may be much stronger than the other so that splitting is not obvious.

We have developed a model of expected Doppler spectra for various microwave and environmental conditions using the wave spectral model of *Donelan et al.* [1985] to compute large-scale velocities. We assumed that waves up to frequencies of 0.35 Hz could be treated as spatially constant over the surface area illuminated by the microwave system, which for the systems used in this study was always less than 4.5 × 7.7 m. These long waves then broadened the Doppler spectrum owing to their temporal variation. Intermediate waves were treated statistically assuming that their line-of-sight-velocity distribution was Gaussian and had a mean square value which could be computed using the spectrum of Donelan et al. Cases for which swell was present on the surface in addition to locally generated seas were handled using the same spectral form but truncated at 0.35 Hz and reduced in magnitude to fix the spectral density at the peak to that of the measured swell.

The directional spectrum $F(\omega, \phi)$ proposed by Donelan et al. is given by

$$\begin{aligned} F(\omega, \phi) &= \tfrac{1}{2}\,\Phi(\omega)\beta\,\operatorname{sech}^2 \beta\phi & |\phi| \le \pi/2 \\ F(\omega, \phi) &= 0 & |\phi| > \pi/2 \end{aligned} \tag{5}$$

where ω is wave angular frequency and ϕ is the wave azimuth angle relative to the direction of propagation of the dominant wave. The parameter β was varied over frequency by *Donelan et al.* [1985] but is given to sufficient accuracy for our purposes by $\beta = 1.9$. The nondirectional spectrum $\Phi(\omega)$ is given for various wind speeds U and peak wave phase speeds c_p by

$$\Phi(\omega) = \alpha g^2 \omega^{-5} (\omega/\omega_p) \exp\{-(\omega_p/\omega)^4\} \gamma^{\Gamma} \tag{6}$$

where $\omega_p = g/c_p$ is the angular frequency at the peak of the spectrum,

$$\alpha = 0.006\,(U/c_p)^{0.55} \qquad 0.83 < U/c_p < 5 \tag{7}$$

$$\begin{aligned} \gamma &= 1.7 & 0.83 < U/c_p < 1 \\ \gamma &= 1.7 + 6.0 \log (U/c_p) & 1 \le U/c_p < 5 \end{aligned} \tag{8}$$

$$\Gamma = \exp\{-(\omega - \omega_p)^2/(2\sigma^2\omega_p^2\} \tag{9}$$

with

$$\sigma = 0.08[1 + 4/(U/c_p)^3] \qquad 0.83 < U/c_p < 5 \tag{10}$$

The ratio U/c_p may be computed from a given fetch x and wind speed using the empirical relationship

$$U/c_p = 11.6(xg/U^2)^{-0.23} \tag{11}$$

where x is in meters, U is in meters per second, and $g = 9.8$ m/s^2. Donelan et al. take U to be the component of wind speed along the direction of propagation of the dominant wave in cases where this does not coincide with the wind direction. We have ignored this small difference here. Using (5) through (11), one may input fetch and wind speed to determine all other parameters and therefore the spectrum itself.

The line-of-sight velocity spectrum produced by the directional spectrum determined in this manner is given by

$$\bar{V}(\omega, \phi_m, \theta_0) = \omega^2 \Phi(\omega) A(\phi_m, \theta_0) \tag{12}$$

where

$$A(\phi_m, \theta_0) = \int_{-\pi/2}^{\pi/2} \tfrac{1}{2}\,\beta[\cos^2\theta_0 + \sin^2\theta_0 \cos^2(\phi_m - \phi) \coth^2(Kd)] \operatorname{sech}^2 \beta\phi \, d\phi \tag{13}$$

Here K is the wave number corresponding to the frequency ω, d is water depth, and ϕ_m is the azimuth angle of the microwave system relative to the dominant wave direction. Multiplication of this spectrum by the frequency resolution, taking the square root, and multiplying by $e^{i\xi}$ where ξ is a random phase assumed to be uniformly distributed yields one realization of the Fourier transform of the time series of line-of-sight velocities, $V(t)$. Transforming yields a realization of the time series itself. In order to insure that the time series is real, it is necessary to make its transform Hermitian, i.e., make the real part even with the imaginary part odd. Accelerations produced by the long waves broaden the microwave Doppler spectrum [*Alpers and Rufenach*, 1979]. The time series of acceleration, $a(t)$, may be computed from $V(t)$ by taking finite differences. Finally, the mean-squared velocity of the intermediate waves may be computed by integrating (12) between the radian frequencies $2\pi(0.35)$ and $\sqrt{gk_B}/5$ where $k_B = 2\pi/\lambda_B$.

In order to model the statistical fluctuations of the velocities of the long waves, the parameter α was drawn from a normally distributed population whose mean was given by (7) and whose variance was one-tenth this mean value. The statistics of the intermediate waves were modeled by drawing individual values of intermediate-scale velocities V_i from a normally distributed population having zero mean and the computed variance (mean square value). Thus for each realization of the surface, the angular frequencies of the advancing (ω_a) and receding (ω_r) Bragg lines were given by

$$\begin{aligned} \omega_a &= \omega_B + 2k_0\left(V_c + V(t) + V_i + \tfrac{1}{2}\,a(t)t^2\right) \\ \omega_r &= \omega_a - 2\omega_B \end{aligned} \tag{14}$$

where k_0 is microwave number, V_c is a mean current line-of-sight velocity, and

$$\omega_B = \sqrt{gk_B + Tk_B^3} = 2\pi f_B \tag{15}$$

Here T (=74 cm^3/s^2) is the ratio of surface tension to water density. Transforming the function

$$f(t) = a_a \exp(i\omega_a t) + a_r \exp[i(\omega_r t + \xi] \tag{16}$$

and taking the modulus squared then gives the expected spectrum for this one realization of the surface. Here a_a and a_r are the amplitudes of the advancing and receding Bragg waves, respectively.

In the code producing modeled spectra, an array size of 64 was chosen for computation of the spectral densities $\bar{V}$. This lead to an array size of 128 for the Fourier transform, i.e., $\sqrt{\bar{V}}$ multiplied by a phase factor and made Hermitian. Thus the time series $V(t)$ was a 128-element array. For each element of this array, $a(t)$ was computed and four estimates of V_i were made. From these values, 512 estimated Doppler spectra could be produced, each of which consisted of two sharp Bragg lines. Two loops were made through this process and resulted in the final Doppler spectra shown below which are composites of 1024 individual spectra.

In order to model the amplitude variation of the advancing and receding Bragg lines with angle between the antenna look direction and the mean wind (or dominant wave direction), we attempted an empirical fit to the L band Doppler spectra to be shown below. The function deemed most acceptable was

$$a_a = 0.4 \cos\phi_m + \sqrt{0.36 - 0.16 \sin^2\phi_m}$$
$$a_r = a_a(\pi - \phi_m) \tag{17}$$

i.e., ϕ_m is replaced by $\pi - \phi_m$ to obtain a_r from a_a. While it is possible, even likely, that this form does not fit higher-frequency spectra well, we have used it in all models. This could introduce a small error in these spectra at azimuth angles other than upwind, downwind, or cross wind, but it is expected to be small.

This model of Doppler spectra does not include the correlation between the intensity of the Bragg wave and the phase of the long or intermediate waves. This effect is normally described by the modulation transfer function and may skew the position of the centroid of the spectrum slightly. Because the dependence of modulation transfer functions on ϕ_m and on differences in direction between wind and waves is incompletely understood at present, this effect, which is second-order in large-scale wave slope, was omitted here.

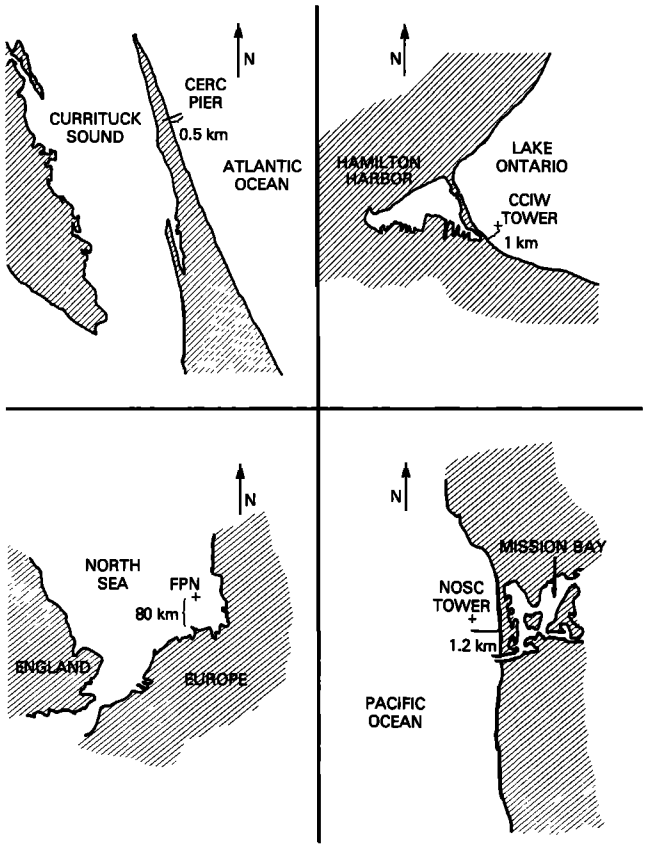

Fig. 2. Locations at which microwave data used to compute Doppler spectra were collected.

3. Comparisons of Measured and Modeled Doppler Spectra

The experimental Doppler spectra reported here were obtained from seven different microwave systems operated over a period of several years. Data were collected at four different sites: (1) the Coastal Engineering Research Center (CERC) pier, which extends into the Atlantic Ocean near Duck, North Carolina; (2) the Canada Centre for Inland Waters (CCIW) tower in Lake Ontario near Burlington; (3) Forschungsplatform NORDSEE (FPN) in the German Bight of the North Sea; and (4) the Naval Ocean Systems Center (NOSC) tower in the Pacific Ocean near San Diego, California. Figure 2 shows the location of these various sites. The microwave systems included instruments operated at L, C,

TABLE 1. Characteristics of the Microwave Systems

Site	Band	Frequency, GHz	Type	Polarization	Two-Way Beamwidth, deg	Height, m	Incidence Angle, deg
CERC	L	1.5	CW	V	8.1	8.5	45
CCIW	K_u	14.0	CW	V/H	4.8	6.5	45
FPN	K_u	14.0	CW	V	4.5	26.0	45
FPN	X	9.3	CW	V	2.3	24.0	40–65
FPN	C	4.3	pulse	V/H	2.4	23.0	54
NOSC	K_u	14.0	CW	V	7.5	14.5	45
NOSC	L	1.5	pulse	H	8.1	18.8	35–54

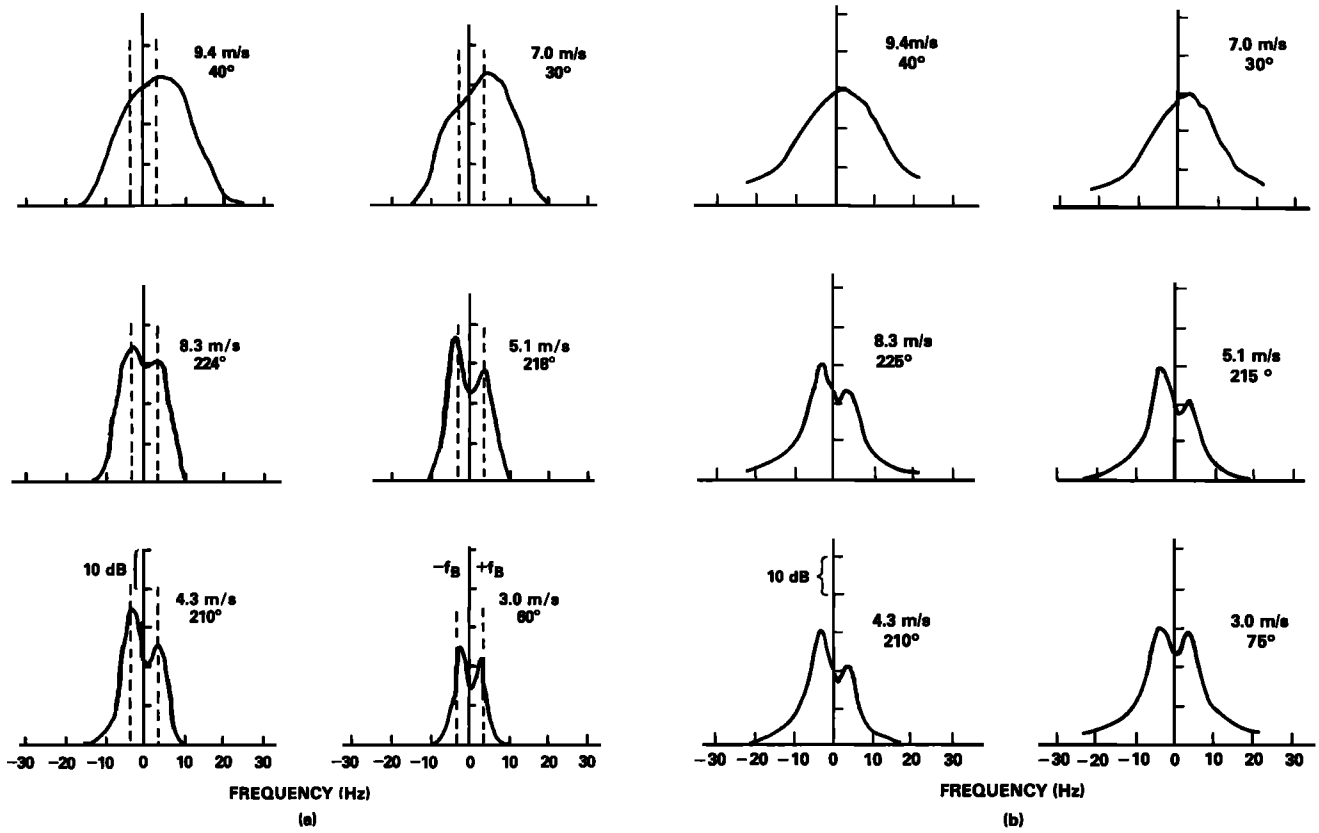

Fig. 3. (*a*) *L* band Doppler spectra obtained at the CERC site for various wind speeds and directions. Antenna azimuth angle is constant at 340° (alongshore to north). Dashed lines indicate expected positions of Bragg peaks. (*b*) Doppler spectra computed with a composite surface model for nearly the same wind speeds and directions as the spectra of Figure 3*a*.

X, and K_u bands; Table 1 gives relevant characteristics of the systems. All systems were coherent and, except for the *L* band system operated on the CERC pier, all were operated in the far field of the antennas. In all cases, the received signals were beat down to a nonzero audio frequency so that folding of the Doppler spectrum was avoided. Doppler spectra were produced from these final audio outputs using Nicolet UA-500A and 440A spectrum analyzers. No attempt was made to calibrate spectral densities absolutely in terms of normalized radar cross sections. Thus only shape and bandwidth information is available from the spectra.

Figure 3*a* shows a series of Doppler spectra obtained with the *L* band system at CERC for different wind speeds and directions and with the antenna directed toward 340°. Each of the spectra shown is an average of 64 individual spectra, each obtained from 4 s of microwave data. Clearly several of the spectra exhibit double peaks similar to the Bragg splittings of Figure 1. For the microwave parameters used here, (1) and (15) yield a Bragg wave frequency f_B of 3.35 Hz. Thus the expected positions of Bragg peaks according to (4) are those indicated by the dashed lines of Figure 3*a*. Agreement with the measured peak positions is very good. To further investigate the correspondence of these spectra to those expected on a composite surface model, we computed expected spectra according to the model of the last section assuming a very low swell and wind wave spectra of *Donelan et al.* [1985] for each fetch and wind speed condition. Characteristics of the low swell were set by matching the resulting significant wave heights and peak frequencies to the measurements made every 6 hours by CERC personnel. Fetches for those cases where the wind was not directed offshore were set to 30 km. The results are shown in Figure 3*b*. The shapes, bandwidths, and occurrence of Bragg splittings in these modeled spectra correspond quite closely with those of the measured spectra.

By comparing the spectra shown in Figure 3*a* which correspond to wind speeds of 7.0, 8.3, and 9.4 m/s one can readily see that at such levels, wind speed is not the determining factor in whether or not Bragg splittings are observed. The primary difference between the conditions under which these spectra were taken was the direction of the wind. Winds from the northeast blow over a long fetch and thus can generate long dominant waves whose orbital velocities are effective in broadening the individual Bragg peaks to make them unresolvable. Winds from 224°, on the other hand, act on the sea surface over a fetch of only about 0.55 km and thus can generate only short dominant waves. Such waves have insufficient orbital velocitites to broaden the Bragg peaks beyond recognition. This indication that wind speed is not the dominant factor determining the width of Doppler spectra argues against the broadening of these spectra being due primarily to a change in the nature of the backscatter with increasing wind up to moderate wind speeds. For instance, if specular scatter or scattering from small-scale breaking waves became dominant at 7 to 9 m/s, one would expect to see broadening irrespective of wind direction. Certainly one would not expect the width of the spectrum to correspond almost exactly to that induced by

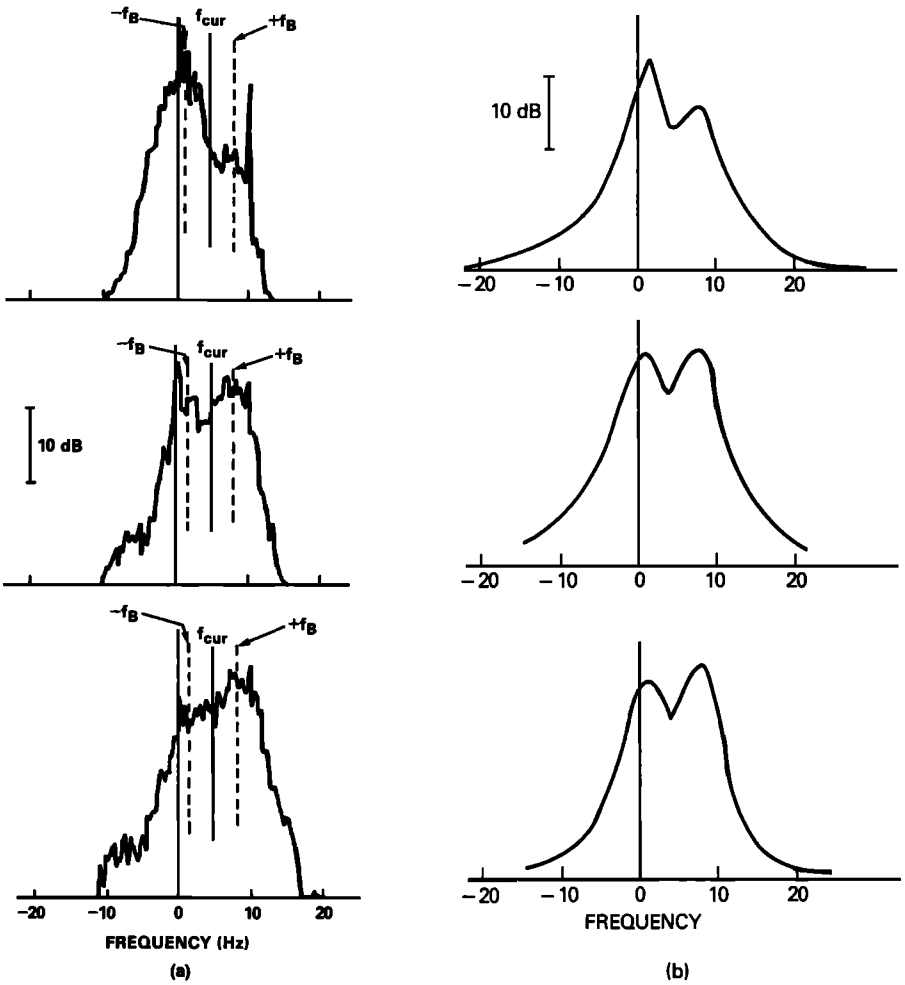

Fig. 4. (*a*) *L* band Doppler spectra obtained at the CERC site for various wind directions when a southerly current was present. Wind velocity was 1 to 2 m/s from 270°, and measured angles between wind and antenna were 110° ± 20°, 90° ± 20°, and 80° ± 20° for top, middle, and bottom spectra, respectively. Solid and dashed lines marked f_{cur} and $\pm f_B$ show expected offset frequency due to the measured 63-cm/s current and the expected positions of Bragg peaks. (*b*) Modeled *L* band Doppler spectra for a current of 63 cm/s, a 1.5-m/s wind speed, and wind-antenna angles of 120°, 90°, and 60° from top to bottom.

Bragg wave advection by orbital velocities. Note that all measurements reported here were made outside the surf zone.

Figure 4 shows measured and modeled spectra collected by the *L* band system at CERC when a significant current was present at the surface. Here only 16 spectra, each obtained using 4 s of data, have been averaged to produce the displayed spectra. We measured the current by timing the speed at which dye floated across the width of the pier. Thus this current includes wind drift effects. The direction of the current was almost directly opposite the look direction of the microwave antenna, and its speed was 63 cm/s. The offset expected from such a current is indicated in Figure 4*a* by the solid vertical line marked f_{cur}; the dashed lines indicate the expected Bragg splittings. Again, good agreement with the measured peak positions is obtained. Wind speed was about 1 to 2 m/s when the spectra of Figure 4*a* were taken. Under these conditions, the wind direction was rather unsteady but was measured to be about 110° ± 20°, 90° ± 20°, and 80° ± 20° away from the antenna look direction for the top, middle, and bottom spectra, respectively. This wind was from approximately 270°; the angle between the wind and antenna look direction was varied by rotating the antenna around a northerly direction. The modeled spectra shown in Figure 4*b* were computed for wind speeds of 1.5 m/s and antenna-wind angles of 120°, 90°, and 60°. The sharp peak evident in the measured spectra near 10 Hz is due to the presence of 60-Hz noise (an artificial 50-Hz offset of zero is not shown).

These results show that Bragg splittings can occur at *L* band under low wind speed conditions with relatively long fetch and under higher wind speed conditions with short fetch. They also indicate, however, that the large-scale velocity and not the wind speed is the factor dominating the occurrence of Bragg splittings. Thus one might expect that situations where significant swell is present in addition to the wind waves would not produce such evident Bragg splittings in Doppler spectra. Figure 5 indicates that this is indeed the case. Figure 5 shows an *L* band spectrum obtained with a 45° incidence angle during the TOWARD experiment on the NOSC tower near San Diego. The antenna was directed toward 270°. In this case, 512 spectra, each obtained from 3.2 s of data, were averaged to obtain the result. In this experiment, as with most of the data reported here, it was

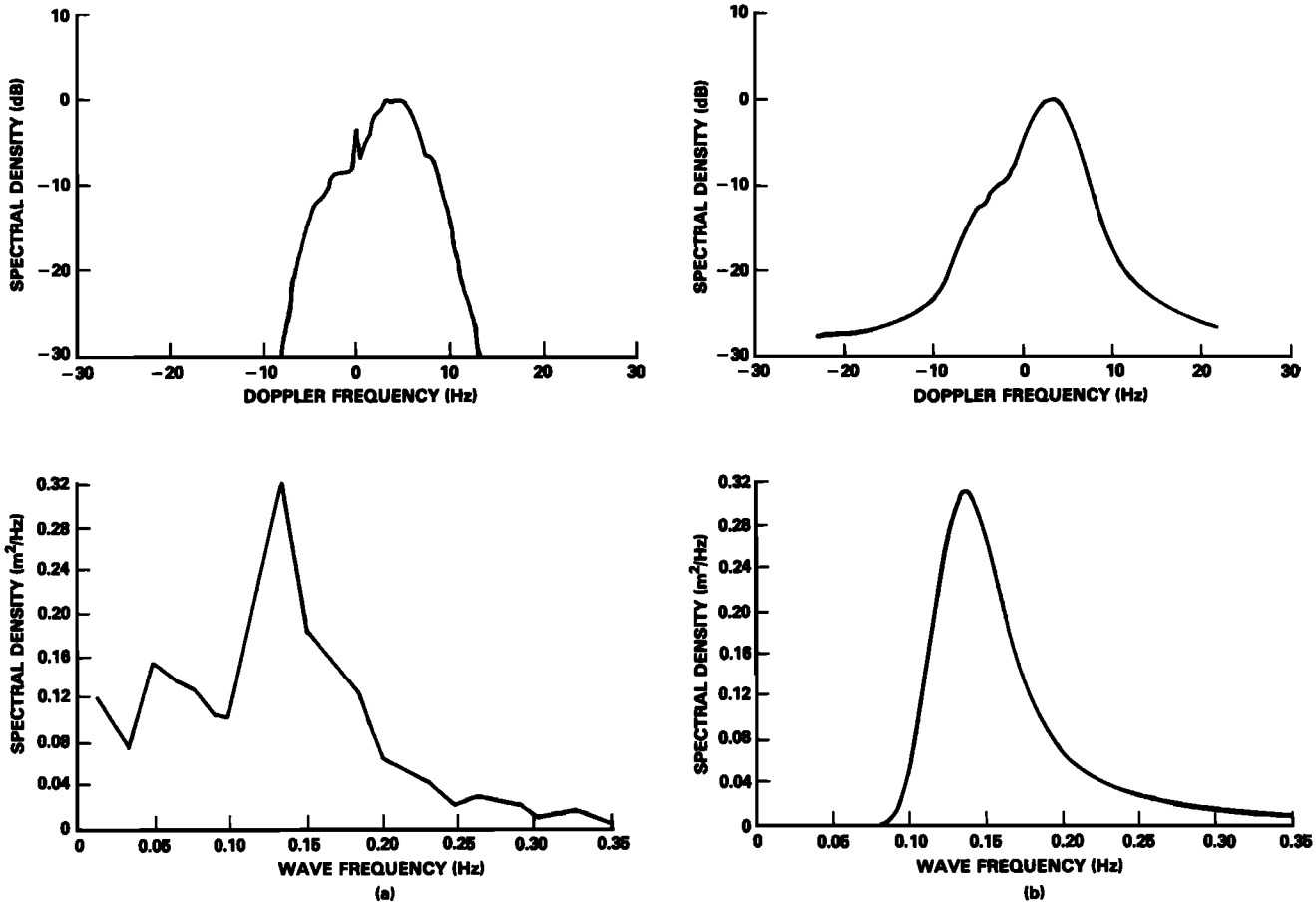

Fig. 5. (*a*) The top graph is an *L* band Doppler spectrum obtained at the NOSC site with a wind velocity of 1.5 m/s from 240°. The microwave antenna pointed toward 270°. The spike at 0 Hz is antenna feedthrough. The bottom graph shows wave spectra obtained from the FM part of the microwave return from which Doppler spectra were computed. (*b*) Modeled Doppler spectrum and corresponding input wave spectrum.

possible to obtain a measurement of the spectrum of dominant waves on the surface directly from the FM output of the radar itself. The method has been described in detail and checked for accuracy by *Plant et al.* [1983]. Figure 5*a* shows this spectrum in the graph below that of the Doppler spectrum; both were measured at a wind velocity of 1.5 m/s from 240°. The dominant feature in the wave spectrum is a peak at about 0.14 Hz which is clearly not a locally generated wind sea. The presence of this swell accounts for the relatively indistinct Bragg splittings in this *L* band Doppler spectrum compared to that shown for a wind speed of 3 m/s in Figure 3 where the swell spectral density was about a factor of 6 lower. Figure 5*b* shows the modeled Doppler spectrum with an input wave spectrum corresponding to the plot below. Once again spectral shape and bandwidth are well modelled by this composite surface picture. The fetch used to compute this model Doppler spectrum was the same as that used to compute the Doppler spectrum at the 3.0-m/s wind speed in Figure 3. The difference in spectral widths must therefore be due to the difference in swell conditions.

These *L* band results indicate that Bragg splittings occur in microwave Doppler spectra under conditions when large dominant waves or swell are not present. To see if such splittings could be observed at higher microwave frequencies, we examined data taken at K_u band in Lake Ontario (the CCIW location) under conditions of short fetch. Figure 6*a* compares measured *L* and K_u band spectra obtained under similar fetch and wind speed conditions. The *L* band spectrum is a repeat of that of Figure 3*a* corresponding to the 8.3-m/s wind speed. The K_u band spectrum is an average of 256 individual spectra, each obtained from 1.6 s of data. It was obtained at CCIW when the wind velocity was 8.0 m/s from 240° and the antenna was directed toward 340°. Under these conditions, the fetch was about 1.0 km, which is comparable to the 0.55 km fetch for the *L* band data. The figure shows that no Bragg splitting occurs at K_u band under these conditions, while it does at *L* band. To see if this is in line with predictions of composite surface theory, we again exercised our model, with the result shown in Figure 6*b*. At both *L* and K_u band, modeled spectra show similar features to measured spectra. In particular, the occurrence or nonoccurrence of Bragg splitting is modeled along with the Doppler bandwidth.

We may readily understand why increasing the microwave frequency causes splittings to disappear by examining equation (4). From this equation, it is apparent that a spread of large-scale line-of-sight velocities ΔV will produce spectral broadening given by

$$(\Delta f)_D = \frac{\Delta V}{\sin \theta_0 \lambda_B} \tag{18}$$

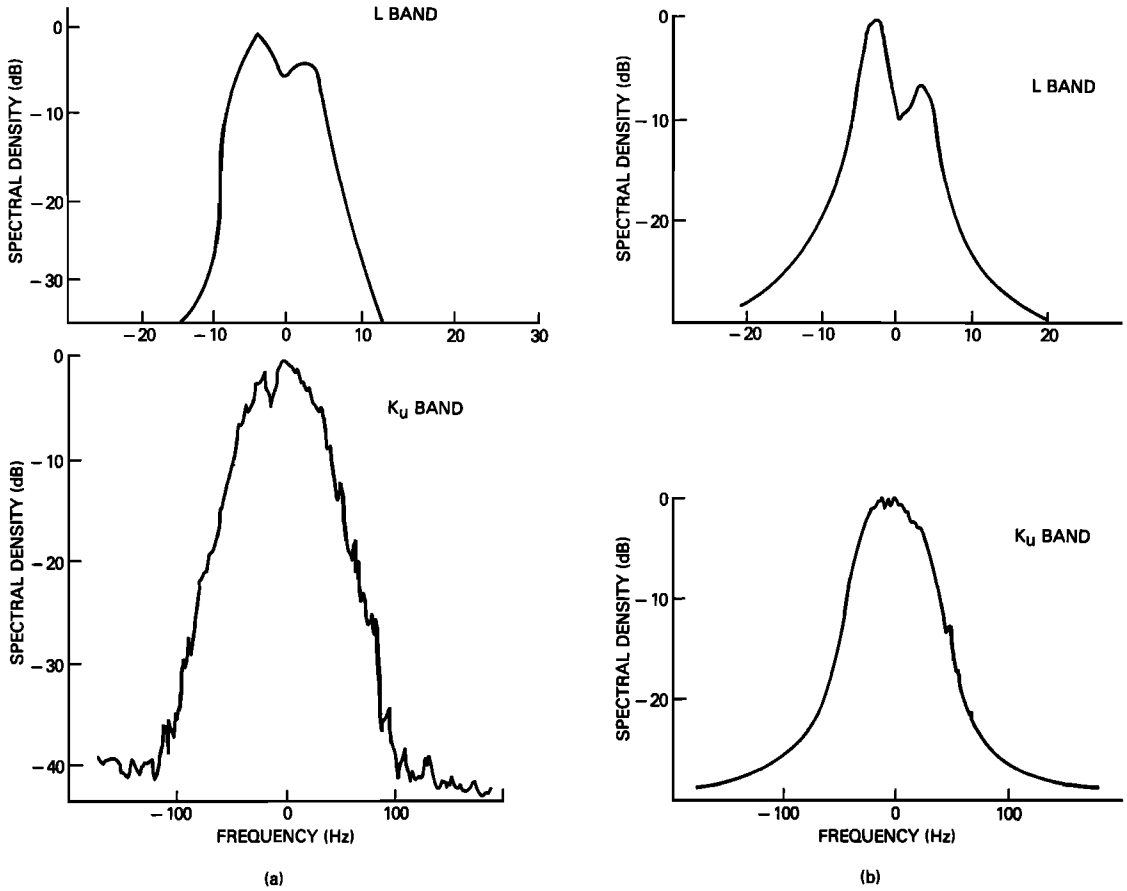

Fig. 6. (*a*) Doppler spectra at L band measured at the CERC site and at K_u band measured at the CCIW site. Wind velocities were 8.3 m/s from 224° and 8.0 m/s from 240°, respectively, while fetches were 0.55 and 1.0 km. In both cases, the antennas were pointed toward 340°. (*b*) Modeled Doppler spectra at L and K_u bands for these conditions.

while the frequency difference between Bragg lines is given by

$$(\Delta f)_B = 2f_B = \frac{2c}{\lambda_B} \tag{19}$$

In order for splitting to be resolved, we require that $(\Delta f)_D < (\Delta f)_B$ or that

$$\frac{\Delta V}{2 \sin \theta_0} < c \tag{20}$$

Under the CERC L band conditions, the Bragg wave has a phase speed of 47 cm/s, while the CCIW K_u band conditions yield a Bragg wave whose speed approaches the minimum of 23 cm/s. Thus for these conditions a spread of large-scale velocities of 45 cm/s, say, would cause resolvable splittings at L band but not at K_u band.

The influence of swell on Doppler bandwidths is also shown to be very significant at these higher microwave frequencies in Figures 7 and 8. These figures again show measured (Figures 7*a* and 8*a*) and modeled (Figures 7*b* and 8*b*) spectra. Top plots are Doppler spectra, while bottom plots are wave spectra. Both measured Doppler spectra were obtained with the K_u band system at the FPN site and are averages of 512 individual spectra, each computed from 0.32 s of data. Both sets of data were taken with wind speeds near 7 m/s but with very different levels of swell present on the surface. In Figure 7, low swell with a period of about 10 s was arriving at the measurement site at an angle of 90° to the antenna look direction. In Figure 8, swell with nearly the same period but with spectral densities more than an order of magnitude higher than those of Figure 7 were arriving at an angle of 40° from the look direction. The effect of the larger swell is obvious in the bandwidths of both the measured and modeled Doppler spectra: those of Figure 8 are nearly twice as large as those of Figure 7. Wind directions in these two figures were, in fact, in such an orientation that they would have tended to broaden the spectrum of Figure 7 more than that of Figure 8 because of Bragg splitting. The wind made an angle of 110° to the antenna look direction in the case of Figure 7 and only 20° for Figure 8. In computing model spectra, a fetch of 40 km was assumed in Figure 7 and 200 km in Figure 8. While this would tend to broaden the spectrum of Figure 8 relative to that of Figure 7, tests indicated that the major source of broadening was indeed the larger swell magnitude in Figure 8. Again, measured and modeled bandwidths agree rather well in both figures.

We have attempted to investigate the effect of incidence angle on Doppler spectra using X band data obtained at the FPN site during the Marine Remote Sensing Experiment (MARSEN). Owing to interference from the tower structure at very low incidence angles, data below 40° incidence angles are missing from this set as from most of our data sets. Nevertheless, several runs were made where incidence

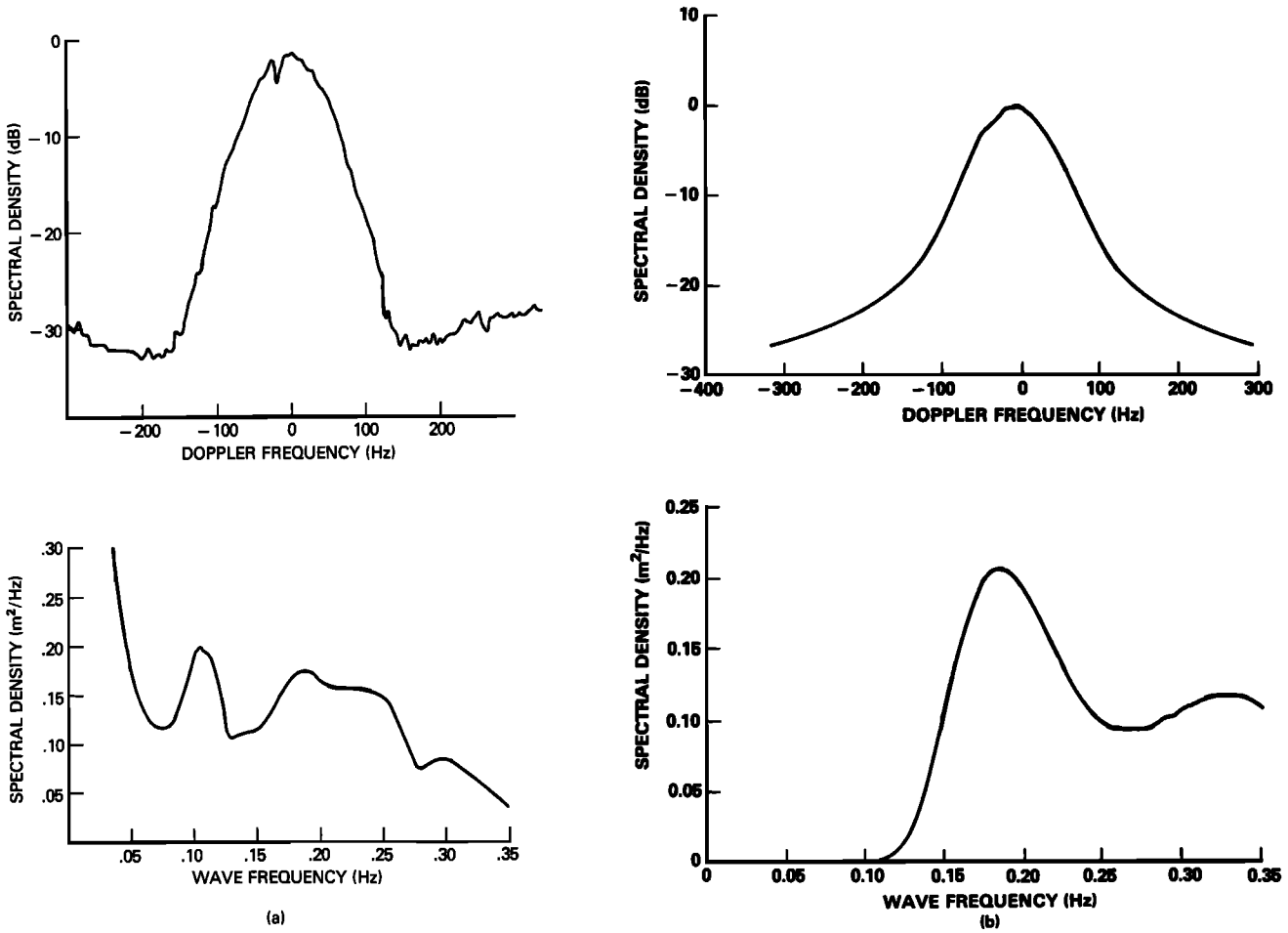

Fig. 7. (*a*) Doppler spectrum at K_u band measured at the FPN site (top) and the wave spectrum at that time (bottom). Wind velocity was 7.0 m/s from 110°. The antennas looked toward 0°. (*b*) Modeled Doppler spectrum for these conditions (top) and the wave spectrum used in the model (bottom).

angles were varied between 40° and 65°. Figure 9*a* shows Doppler spectra obtained on one of these runs when the wind speed varied between 6.5 and 9 m/s while its direction stayed near 345°. The antennas were pointed toward 310°. These spectra are averages of 512 individual spectra, each computed from 0.4 s of data. Figure 9*b* shows corresponding modeled spectra computed assuming only a wind sea to be present. The data and model both show little systematic variation in Doppler bandwidth with incidence angle. This is not surprising, since waves in the German Bight under these conditions are little influenced by the bottom, so that orbits of water parcels induced by the waves are nearly circular. Thus the spread of line-of-sight velocities induced by these waves will be nearly independent of viewing angle. Since the Bragg wavelength and therefore frequency also change little over the range of incidence angles presented here, little change in Doppler bandwidth should be expected on a composite surface model (see equation (4)).

Figure 10 summarizes the accuracy of the model in obtaining the measured Doppler bandwidth; the data shown in the figure are also given in Table 2 along with wind velocities and antenna directions. We have chosen to compare bandwidths at a level 10 dB below the maximum of the spectrum. Other levels could be chosen but make little difference in the nature of the results. Figure 10 shows that under most conditions the model predicts measured bandwidths to within 15% but that it is usually biased low. Only one point at a very high bandwidth falls significantly outside this range. It is FPN K_u band data taken at a wind speed of 30 m/s. The fact that the highest bandwidth is that at which the model badly underpredicts the bandwidth is probably coincidence: we happened to get wind speeds this high only when K_u band data were being taken. It is reasonable to expect that bandwidths at lower microwave frequencies, i.e., lower bandwidths, would also be underpredicted by the model at very high wind speeds. This probably indicates the increasing importance of other scattering mechanisms at these high wind speeds.

As was pointed out above, aside from the high wind speed point, modeled bandwidths generally fall within 15% of measured bandwidths. In view of the uncertainties of modeling long-wave spectra, this agreement is rather satisfying. It is important to note that such agreement would not have occurred if orbital velocities of large-scale waves alone caused the spectral width; the extra bandwidth contributed by the splitting of advancing and receding Bragg waves is very necessary. For the assumed angular dependence of Bragg wave amplitude given by (17), Bragg splitting will be an important effect on 10-dB Doppler bandwidths any time the wind makes an angle of more than 45° with the antenna

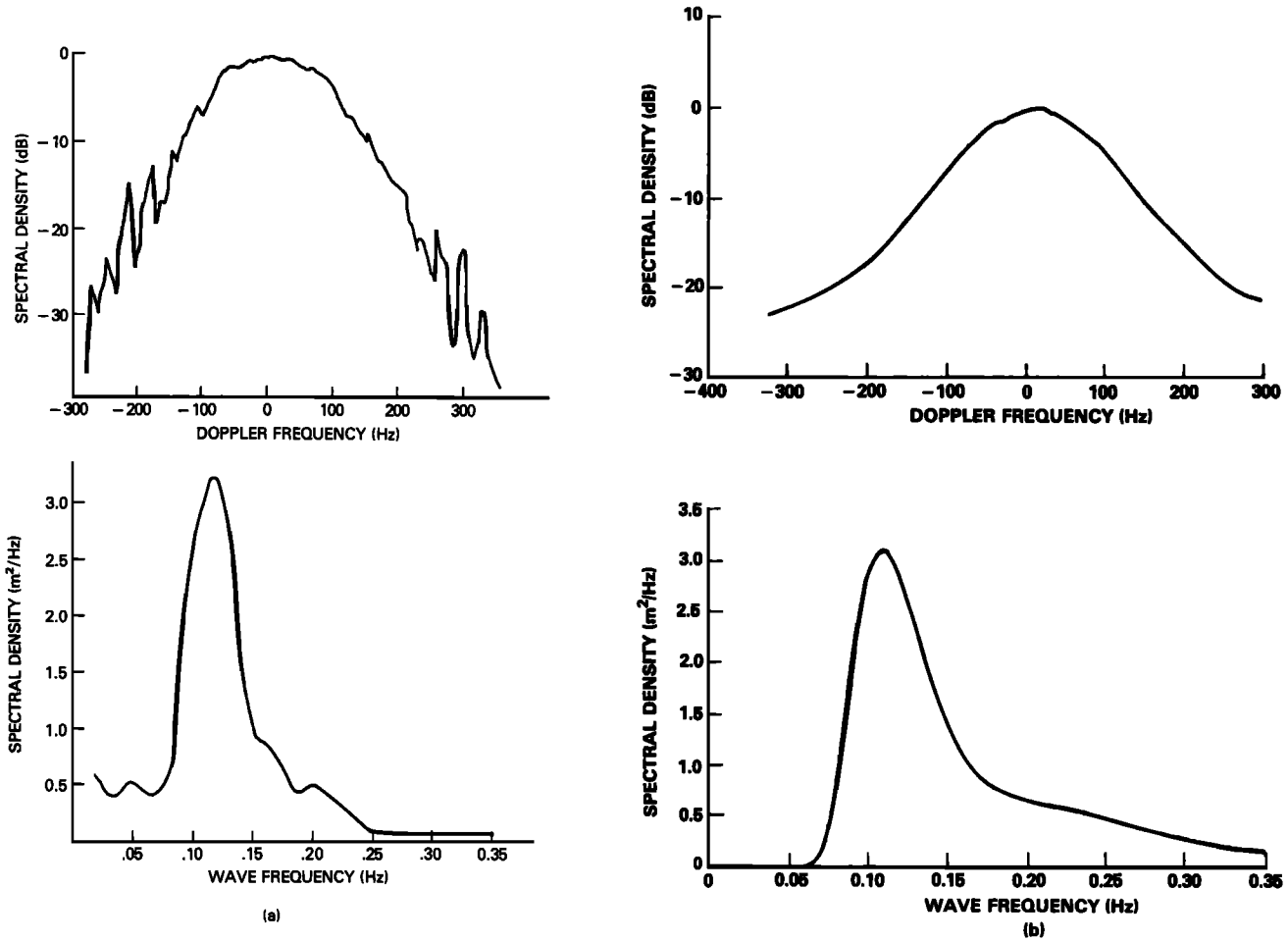

Fig. 8. Same as Figure 7 but for higher swell conditions. Wind velocity was 6.7 m/s from 340° and the antennas were pointed toward 300°.

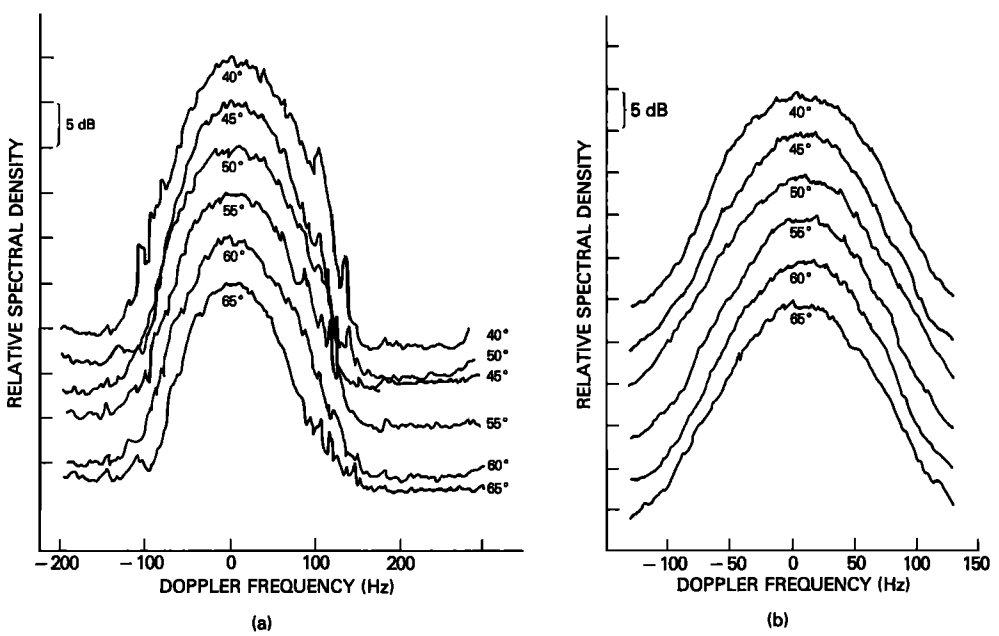

Fig. 9. (*a*) Doppler spectra at *X* band measured at the FPN site for the indicated incidence angles. Wind speeds for spectra from top to bottom were 8.0, 6.5, 9.0, 7.0, 9.0, and 7.5 m/s. Wind directions were from 350° ± 15° while the antennas were directed toward 310°. (*b*) Modeled Doppler spectra for the same conditions.

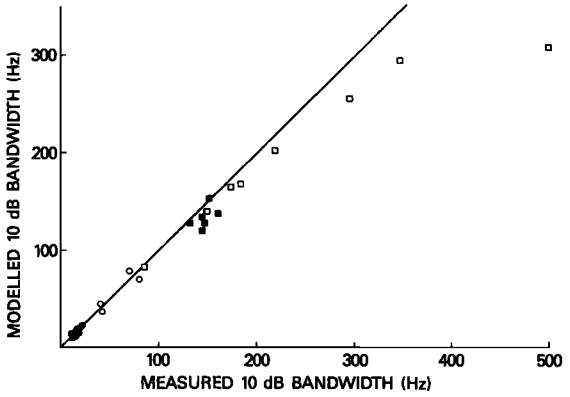

Fig. 10. Modeled Doppler bandwidths versus measured bandwidths for all data analyzed in this study. Symbols correspond to the following different microwave frequencies: solid circles, L band; open circles, C band; solid squares, X band; open squares, K_u band. Bandwidth shown are full widths 10 dB below the maximum spectral density. See Table 1 for a listing of these data.

look direction. Such conditions occurred more than half the time for the data displayed in Figure 10. The magnitude of the splitting varies with microwave frequency and for parameters reported here amounts to about 6 Hz at L band, 13 Hz at C band, 25 Hz at X band, and 32 Hz at K_u band. Subtracting such amounts from the modeled bandwidths shown in Figure 10 would substantially reduce the agreement with measured bandwidths.

4. Discussion and Conclusion

The effect of these Bragg splittings on Doppler bandwidths is important to discussions of ocean wave imagery by synthetic aperture radars (SAR). In such imagery, an important parameter governing the relationship between spectra of SAR images and spectra of ocean surface waves is the coherence time. This is defined in such a manner that it is almost exactly the inverse of the 10-dB Doppler bandwidth of sea return in the absence of long waves [*Alpers et al.*, 1981]. Thus the coherence time must vary with angle between the wind and the SAR look direction due to the variation in advancing and receding Bragg wave amplitudes. For imagery of wind-generated, azimuthally travelling waves, the splitting can contribute on the order of half the bandwidth of the spectrum thus reducing the coherence time by nearly a factor of 2. Unfortunately, at least two studies have indicated that coherence times on the order of 0.025 s are necessary to deduce proper wave spectra from L band SAR imagery of azimuthal waves using present SAR imaging theory [*Alpers et al.*, 1986; *Macklin and Cordey*, 1989]. This corresponds to 10-dB bandwidths at L band of 40 Hz, far greater than any measured or modeled in this study. Thus this study does not support a decrease in coherence time as a method for deducing more accurate wave spectra from SAR imagery.

This study does provide much support for the Bragg-scattering/composite-surface type of model which is usually assumed for sea return in SAR imaging models. The observed splittings of L band Doppler spectra and the fact that for wind speeds below about 25 m/s, Doppler bandwidths for

TABLE 2. Summary of Measured and Modeled 10-dB Bandwidths

Site	Band	Wind Speed, m/s	Wind Direction, deg	Antenna Direction, deg	Measured Bandwidth, Hz	Modeled Bandwidth, Hz
TOWARD	L	6.3	202	270	22.0	22.5
TOWARD	L	0.6	23	290	15.2	12.5
TOWARD	L	1.5	240	270	12.0	10.7
TOWARD	L	1.9	81	60	18.8	16.1
TOWARD	L	5.9	231	250	18.8	19.4
TOWARD	L	2.4	249	250	14.5	14.8
CERC	L	9.4	40	340	19.1	18.4
CERC	L	7.0	30	340	15.8	15.8
CERC	L	5.1	218	340	10.5	10.5
CERC	L	8.3	224	340	11.6	12.1
FPN	C	21.3	250	290	79	70
FPN	C	9.5	270	315	70	79
FPN	C	6.5	235	290	40	45
FPN	C	2.8	175	225	42	37
FPN	X	7.5	340	310	126	128
FPN	X	9.0	360	310	147	148
FPN	X	7.0	345	310	144	121
FPN	X	9.0	345	310	158	137
FPN	X	6.5	340	310	132	128
FPN	X	8.0	335	310	144	135
NOSC	K_u	8.5	239	315	183	168
NOSC	K_u	7.2	252	315	173	165
FPN	K_u	30.3	265	300	498	324
FPN	K_u	20.0	280	300	346	303
FPN	K_u	6.7	320	300	295	268
FPN	K_u	15.4	210	300	219	211
FPN	K_u	7.0	110	0	149	144
CCIW	K_u	8.0	240	340	87	91

microwave frequencies up to K_u band can be predicted to within 15% by such a model supports the contention that Bragg scattering is probably the most important source of microwave sea return at intermediate incidence angles. From these Doppler spectra alone, it is not possible to assign a value to the percent of sea return which can be attributed to Bragg scattering because absolute spectral densities were not measured. Even if such calibration had been accomplished, the need to know accurate levels of Bragg wave spectral densities which has mentioned in the introduction would still remain. Until such time that accurate measurements of Bragg wave spectral densities in the wave number domain can be made, the best that can be said is that Doppler spectra behave in a manner consistent with the assumption that Bragg scattering is the major source of microwave sea return at intermediate incidence angles and low to moderate wind speeds.

Acknowledgments. This work was supported by the Naval Research Laboratory's Basic Research Program and by the Contract Research Department of the Office of Naval Research. This paper is WHOI contribution 7031.

REFERENCES

Alpers, W. R., and C. L. Rufenach, The effect of orbital motions on synthetic aperture radar imagery of ocean waves, *IEEE Trans. Antennas Propag.*, *AP-27*, 685–690, 1979.

Alpers, W. R., D. B. Ross, and C. L. Rufenach, On the detectability of ocean surface waves by real and synthetic aperture radar, *J. Geophys. Res.*, *86*, 6481–6498, 1981.

Alpers, W., C. Bruening, and K. Richter, Comparison of simulated and measured synthetic aperture radar image spectra with buoy-derived ocean wave spectra during the Shuttle Imaging Radar B mission, *IEEE Trans. Geosci. Remote Sens.*, *GE-24*, 559–566, 1986.

Barrick, D. E., J. M. Headrick, R. W. Bogle, and D. D. Crombie, Sea backscatter at HF: Interpretation and utilization of the echo, *Proc. IEEE*, *62*, 673, 1974.

Bass, F. G., I. M. Fuks, A. I. Kalmykov, I. E. Ostrovsky, and A. D. Rosenberg, Very high frequency radiowave scattering by a disturbed sea surface, II, Scattering from an actual sea surface, *IEEE Trans. Antennas Propag.*, *AP-16*, 560–568, 1968.

Donelan, M. A., and W. J. Pierson, Jr., Radar scattering and equilibrium ranges in wind-generated waves with application to scatterometry, *J. Geophys. Res.*, *92*, 4971–5029, 1987.

Donelan, M. A., J. Hamilton, and W. H. Hui, Directional spectra of wind-generated waves, *Philos. Trans. R. Soc. London, Ser. A*, *315*, 509–562, 1985.

Durden, S. L., and J. F. Vesecky, A physical radar cross section model for a wind-driven sea with swell, *IEEE J. Oceanic Eng.*, *OE-10*, 445–451, 1985.

Guinard, N. W., J. T. Ransone, Jr., and J. C. Daley, Variation of the NRCS of the sea with increasing roughness, *J. Geophys. Res.*, *76*, 1525–1538, 1971.

Hasselmann, K., R. K. Raney, W. J. Plant, W. Alpers, R. A. Shuchman, D. R. Lyzenga, C. L. Rufenach, and M. J. Tucker, Theory of synthetic aperture radar ocean imaging: A MARSEN view, *J. Geophys. Res.*, *90*, 4659–4686, 1985.

Kitaigorodski, S. A., On the theory of the equilibrium range in the spectrum of wind-generated gravity waves, *J. Phys. Oceanogr.*, *13*, 816–827, 1983.

Kwoh, D. S. W., and B. M. Lake, Microwave backscattering from short gravity waves: A deterministic, coherent and dual-polarized laboratory study, *Rep. 37564-6001-UT-00*, pp. 75, TRW, Redondo Beach, Calif., 1983.

Kwoh, D. S. W., and B. M. Lake, A deterministic, coherent, and dual-polarized laboratory study of microwave backscattering from water waves, I, Short gravity waves without wind, *IEEE J. Oceanic Eng.*, *OE-9*, 291–308, 1984.

Larson, T. R., and J. W. Wright, Wind-generated gravity-capillary waves: Laboratory measurements of temporal growth rates using microwave backscatter, *J. Fluid Mech.*, *70*, 417–436, 1975.

Lee, H. Y., Doppler measurements of the effect of gravity waves on wind-generated ripples, *J. Fluid Mech.*, *81*, 225–240, 1977.

Macklin, J. T., and R. A. Cordey, Ocean-wave imaging by synthetic aperture radar: Results from the SIR-B experiment in the N.E. Atlantic, *IEEE Trans. Geosci. Remote Sens.*, *27*, 28–35, 1989.

Phillips, O. M., Spectral and statistical properties of the equilibrium range in wind-generated gravity waves, *J. Fluid Mech.*, *156*, 505–531, 1985.

Plant, W. J., A two-scale model of short wind-generated waves and scatterometry, *J. Geophys. Res.*, *91*, 10,735–10,749, 1986.

Plant, W. J., and J. W. Wright, Growth and equilibrium of short gravity waves in a wind-wave tank, *J. Fluid Mech.*, *82*, 767–793, 1977.

Plant, W. J., and J. W. Wright, Spectral decomposition of short gravity wave systems, *J. Phys. Oceanogr.*, *9*, 621–624, 1979.

Plant, W. J., and J. W. Wright, Phase speeds of upwind and downwind traveling short gravity waves, *J. Geophys. Res.*, *85*, 3304–3310, 1980.

Plant, W. J., W. C. Keller, and A. Cross, Parametric dependence of ocean wave-radar modulation transfer functions, *J. Geophys. Res.*, *88*, 9747–9756, 1983.

Valenzuela, G. R., and M. B. Laing, Study of Doppler spectra of radar sea echo, *J. Geophys. Res.*, *75*, 551–563, 1970.

Wright, J. W., Backscattering from capillary waves with application to sea clutter, *IEEE Trans. Antennas Propag.*, *AP-14*, 749–754, 1966.

Wright, J. W., A new model for sea clutter, *IEEE Trans. Antennas Propag.*, *AP-16*, 217–223, 1968.

Wright, J. W., and W. C. Keller, Doppler spectra in microwave scattering from wind waves, *Phys. Fluids*, *14*, 466–473, 1971.

W. C. Keller, U.S. Naval Research Laboratory, Washington, DC 20375.

W. J. Plant, Woods Hole Oceanographic Institution, Woods Hole, MA 02543.

(Received September 8, 1988;
accepted December 13, 1988.)